Microcirculation Volumetric Flow Assessment Using High-Resolution, Contrast-Assisted Images

Chih-Kuang Yeh, *Member, IEEE*, Sheng-Yi Lu, and Yung-Sheng Chen, *Member, IEEE*

***Abstract*—To improve the resolution of contrast-assisted imaging systems, we previously developed a 25-MHz microbubbles-destruction/replenishment imaging system with a spatial resolution of 160 × 160 μm. The goal of the present study was to propose a new approach for functionally evaluating the microvascular volumetric blood flow based on this high-frequency, ultrasound imaging system. The approach includes locating the perfusion area and estimating the blood flow velocity therein. Because the correlation changes between before and after microbubble destruction in two adjacent images, a correlated-based approach was introduced to detect the blood perfusion area. We also have derived a new sigmoid-based model for characterizing the microbubbles replenishment process. Two parameters derived from the sigmoid-based model—the rate constant and inflection time—were adopted to evaluate the blood flow velocity. This model was validated using both simulations and *in vitro* experiments for mean flow velocities ranging from 1 to 10 mm/s, which showed that the model was in good agreement with simulated and measured microbubble-replenishment time-intensity curves. The results indicate that the actual flow velocity is highly correlated with the estimates of the rate constant and the reciprocal of the inflection time. B-mode imaging experiments for mean flow velocities ranging from 0.4 to 2.1 mm/s were used to assess the volumetric flow in the microcirculation. The results indicated the high correlation between the actual volumetric flow rate and the product of the estimated perfusion area and rate constant, and the reciprocal of the inflection time. We also found that the boundary of the microbubble destruction volume significantly affected estimations of the flow velocity. The perfusion area can be located, and the corresponding flow velocity can be estimated simultaneously in a one-stage, microbubble-destruction/replenishment process, which makes the assessment of the volumetric blood flow in the microcirculation feasible using a real-time, high-frequency ultrasound system.**

I. Introduction

Microvascular changes occur in many disease states, including cancer and diabetes. The neovasculature formed through the angiogenetic process during cancer is critical to tumor proliferation and metastasis [1]. Current treatments such as antiangiogenic therapies focus on controlling angiogenesis and reducing tumor perfusion. There is considerable evidence that the prognosis is linked to the specific pattern of microvascular morphology [2], [3]. Because assessments of the microvascular status can yield clinically significant information, assessing the volumetric flow in the microcirculation would be of particular interest in tumor diagnosis and prognosis.

However, there are several limitations to using conventional medical ultrasound to evaluate microvascular changes. The first problem is that the spatial resolution of conventional Doppler ultrasound systems operating at 2–10 MHz is insufficient to detect smaller vessels within the microcirculation. Typical vessel sizes and flow velocities within the microcirculation are in the ranges of 5 to 200 μm and 0.1 to 10 mm/s, respectively [4], [5]. The resolution and blood backscattering coefficient improve with increasing ultrasound frequency. This prompted the creation of high-frequency ultrasound imaging systems (>15 MHz), which provide spatial resolutions of 50–200 μm. Applications of high-frequency ultrasound include noninvasive imaging of small-scale, superficial structures such as the skin, the anterior chamber of the eye, and mouse embryos [6]–[9]. Operating in color Doppler and power Doppler imaging modes at 40 MHz provides spatial resolutions down to 40 μm, yielding the capability of mapping blood velocity and the power of Doppler signals from moving red blood cells [10]–[12]. These previous studies and the described systems have not been capable of evaluating the flow in the entire microcirculation, and vessels with diameters of less than 40 μm were not detectable.

The second problem of conventional ultrasound systems is the weak backscattered echo from small vessels. Ultrasound contrast agents (UCAs) are used to improve the sensitivity of the ultrasound flow mapping system, allowing arterioles, venules, and capillaries to be investigated. UCAs are shell-encapsulated microbubbles that enhance the backscattered echoes from blood. Sonication by low-frequency ultrasound pulses can result in UCA bubbles fragmenting into smaller bubbles and/or diffusion of the encapsulated gas [13]–[15], which is utilized by contrast-assisted imaging methods to evaluate flow velocity and blood perfusion, and to improve the blood-to-tissue image contrast. Frinking *et al.* [16] suggested that a burst of ultrasound could be used to destroy the microbubbles. Then

Manuscript received March 15, 2007; accepted August 13, 2007. The authors would like to acknowledge National Science Council of Republic of China for providing support (NSC 95-2314-B-007-007-MY3) and the reviewers for valuable comments.

C.-K. Yeh and S.-Y. Lu are with the Department of Biomedical Engineering and Environmental Sciences, National Tsing Hua University, Hsinchu, Taiwan (e-mail: ckyeh@mx.nthu.edu.tw).

Y.-S. Chen is with the Department of Electrical Engineering, Yuan Ze University, Chungli, Taiwan.

Digital Object Identifier 10.1109/TUFFC.2008.618

the microbubbles could be distinguished from the background tissue by measuring the decorrelation between the changes in the intensity of echo signals between before and after the ultrasound burst.

The well-known, contrast-assisted imaging methods can be considered as microbubble-destruction/replenishment techniques [17]. Following destruction of microbubbles with lower frequency pulses, the intact microbubbles flowing into the sample volume can be monitored over time to produce a local estimate of flow velocity in a region of interest (ROI). The graphical representation of the gradual increase in the echo intensity due to the replenishment of microbubbles as a function of time is typically referred to as the time-intensity curve (TIC). Wei *et al.* [17] proposed a growing monoexponential function to characterize TICs and to assess the blood flow velocity in the myocardium. Their model predicts that the intensity of the received echo increases exponentially over time, before saturating. Related studies include assessments of myocardial perfusion, renal flow, cerebral blood perfusion, and tumor perfusion [18]–[24].

Certain TICs detected in cerebral [21] and renal tissue perfusion [25], [26] were not consistent with the monoexponential model, instead requiring a sigmoid-based model for good agreement. Lucidarme *et al.* [26] assumed that the fraction of microbubbles that fragmented prior to replenishment into the ROI resulted in TICs similar to sigmoidal curves. They also demonstrated the conditions for the transition between sigmoid- and monoexponential-based model behaviors in a multicompartment model. Hudson *et al.* [27] introduced an analytic replenishment model to characterize TICs in different hemodynamic and beam geometry conditions that took the hemodynamics, vascular morphology, acoustics field distribution, and microbubble properties into consideration. Arditi *et al.* [28] provided a new formalism for the microbubble-destruction/replenishment perfusion-quantification approach that accounted for the spatial distribution of the transmit/receive ultrasound beam in the elevation plane. They assumed that the sigmoid-shaped TIC was formed by a linear combination of elementary cumulative normal distribution functions weighted by the probability density function of flow transit times within the region. Krix *et al.* [29] presented a hyperbolic model for quantifying the replenishment of microbubbles. This model relies on a physiological and consistent description of refilling, and it takes into account the variability of blood flow velocities in a given volume of tissue *in vivo*.

To improve the resolution of contrast-assisted imaging systems, we previously developed a 25-MHz microbubble-destruction/replenishment imaging system with a spatial resolution of 160×160 μm [30]. The goal of the present study is to propose a new approach for functionally evaluating the microvascular volumetric blood flow based on this high-frequency ultrasound imaging system. The approach includes locating the perfusion area and estimating the blood flow velocity therein. Here we introduce a correlated-based method for locating the blood perfusion area, and a new sigmoid-based model for characterizing the UCA-replenishment process. The relationship between the progressive arrival of UCAs at a specific location within the sample volume and corresponding TIC is characterized. Two parameters derived from the sigmoid-based model—the rate constant and inflection time—are adopted to evaluate the blood flow velocity. Both simulations and *in vitro* experiments were performed to validate the proposed sigmoid-based model. The perfusion area (PA) can be located, and the corresponding flow velocity (v) can be estimated simultaneously in a one-stage microbubble-destruction/replenishment process, which makes the assessment of volumetric blood flow (S) in the microcirculation feasible, and is given by:

$$S = v \times PA. \tag{1}$$

Here we first derive sigmoid-based TICs, then detail the approach used to locate the perfusion area, describe the *in vitro* experimental system for microcirculation flow estimation, then summarize the results of simulations and *in vitro* experiments.

II. Methodology

A. Sigmoidal Function and Time-Intensity Curves

Infusion with a contrast agent at a constant rate and concentration will produce a steady-state concentration throughout the circulation after a certain period of time. The subsequent local application of high-pressure ultrasound pulses will destroy microbubbles within a confined volume, and intact microbubbles will enter this volume at a rate determined by the flow velocity and vessel topology. Nondestructive imaging sequences were used to determine the changes in the backscattered echo intensity as a function of time (i.e., the TIC) within this volume. Wei *et al.* [17] proposed a growing monoexponential model to describe the echo intensities resulting from the summed contributions of all microbubbles within the sample volume.

Assuming a linear system, the flow is assessed by convolving the input function following destruction (modeled as a scaled unit-step function) with the beam response function (modeled as a scaled Gaussian function). The nonuniform signal intensity resulting from flow velocities and backscattered amplitudes of the echoes of microbubbles entering the sample volume are approximated by a sigmoidal function [as in Fig. 1(a)]. The equation for the received signal intensity ($f(t)$) as a function of time after microbubbles destruction is given by:

$$f(t) = A\left(\frac{1}{1+e^{-\alpha(t-c)}}\right), \tag{2}$$

where A is the steady-state intensity of the received echo, α is the rate constant for the rise of the sigmoidal function, and c is the time interval from the start to the inflection point of the sigmoidal function (i.e., the inflection

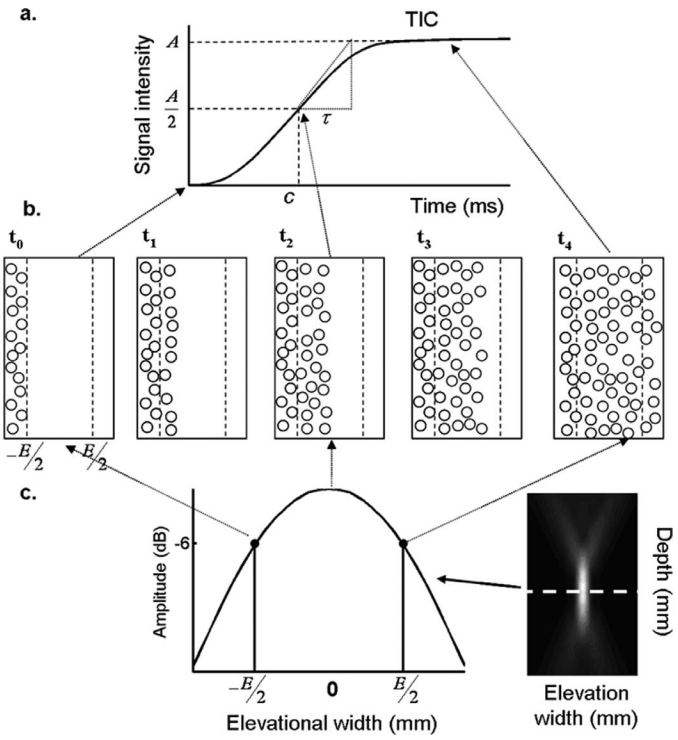

Fig. 1. (a) Sigmoid-based time-intensity curve model. (b) Diagrams of the time course of microbubble replenishment. (c) Elevational beam pattern of the imaging transducer.

time). Diagrams of the time course of microbubble replenishment through the imaging plane are shown in Fig. 1(b). Our previous work used a system with a 1-MHz cylindrically focused transducer for microbubble destruction and a 25-MHz spherically focused transducer for high-resolution imaging [30]. Because the use of these transducers results in the destruction sample volume being much larger than the imaging volume, we assumed that replenishment with intact microbubbles begins at the boundary of the −6-dB elevational beam width (i.e., $\pm E/2$) of the imaging transducer. The acoustic beam pattern of the imaging transducer along the elevation direction is shown in Fig. 1(c).

When the microbubble concentration is restored to 50% in the sample volume [i.e., at t_2 in Fig. 1(b)], the time-intensity relationship corresponds to the inflection point of the sigmoidal function. The tangent slope of the TIC increases with time before the inflection point due to the increasing intensity of the ultrasound beam, and decreases thereafter. The flow velocity (v) can be calculated as:

$$v = \frac{E/2}{c}. \tag{3}$$

The tangent slope at the inflection point is given by:

$$\left.\frac{\mathrm{d}f}{\mathrm{d}t}\right|_{t=c} = A\alpha \left.\frac{e^{-\alpha(t-c)}}{\left(1+e^{-\alpha(t-c)}\right)^2}\right|_{t=c} = \frac{A\alpha}{4}. \tag{4}$$

As shown in Fig. 1(a), the slope also is equal to $(A/2)/c$, hence:

$$c = \frac{2}{\alpha}. \tag{5}$$

From (5), (3) can be rewritten as:

$$v = \frac{\alpha}{4}E. \tag{6}$$

The size of the microbubble fragmentation volume varies with the sonication parameters of the destruction pulses and the concentration at which bubbles are infused, which makes it challenging to estimate the absolute flow velocity from (6). However, assuming that E is a constant makes estimation of the relative flow velocity feasible and proportional to $\alpha(s^{-1})$ and $1/c(s^{-1})$. Therefore, (1) can be rewritten as:

$$S \propto \alpha \cdot PA, \tag{7}$$

$$S \propto \frac{1}{c} \cdot PA. \tag{8}$$

B. Model Fitting and the Integrated Time-Intensity Curve

TICs typically have high variances due to the various flow velocities in different vessels within the sample volume, echo decorrelations in the microbubble-replenishment process, cardiac pulsatility, and variability in bubble scattering. The use of high-resolution ultrasound results in a small number of microbubbles within a single ROI. Therefore, a high noise level can be present in estimates of flow based on the movement of these contrast agents. Although it is possible to directly estimate A, α, and c from (2), the variance is high and the presence of false minima can produce large errors. To reduce the influence of noise on time-intensity measurements, we used an integrated TIC (ITIC) method to reduce the effects of parameter variability on the flow estimation [30]. A modified method is adopted here for estimating A, α, and c from the ITIC.

The ITIC of a sigmoidal function is given by:

$$\begin{aligned} I(t) &= \int_0^t f(\tau)d\tau \\ &= \frac{A}{\alpha}\log\left(1+e^{-\alpha(t-c)}\right) + \left(At - \frac{A}{\alpha}\log\left(1+e^{\alpha c}\right)\right), \end{aligned} \tag{9}$$

where log denotes the natural logarithm and $I(t)$ is the integration of (2) from zero to t, which is the time elapsed from microbubble destruction. If $\alpha(t-c)$ being sufficiently large arrives at advanced time with respect to microbubble destruction, (9) can be simplified to:

$$I(t) \approx At - \frac{A}{\alpha}\log\left(1+e^{\alpha c}\right). \tag{10}$$

Eq. (10) implies that the ITIC is approximately linear occurs at advanced time with respect to microbubble destruction, and A can be estimated from (10) by linear fitting to $I(t)$, where the slope corresponds to the estimate of A.

The ITIC of a sigmoidal function defined in (10) is divided into different values of t according to:

$$I'(t) = \frac{\int_0^t f(\tau)d\tau}{t} = \frac{A}{\alpha t}\log\left(\frac{1+e^{-\alpha(t-c)}}{1+e^{\alpha c}}\right) + A, \tag{11}$$

where t is the time elapsed from bubble destruction. Note that in the limit $t \to 0$, $I'(t) \to 0$, and in the limit $t \to \infty$, $I'(t) \to A$. $I'(t)$ is inherently less noisy than the TIC because it is a running average of the TIC. With the estimated value of A from (10), the estimates of α and c can be jointly obtained from curve fitting to the ITIC model in (11). Note that the definition of the ITIC used throughout this paper corresponds to the time-averaged ITIC shown in (11).

C. Locating the Perfusion Area

A correlation-based approach (CBA) was used to detect the presence of microbubbles (i.e., the perfusion area) [16], [31]. The CBA is based on the correlation changes between before and after microbubble destruction in two received images/data sets. The correlation analysis was performed on short, sliding, and overlapping sampling windows of the ultrasound received images/data set in this study. Here we use two RF signals to illustrate the principle of CBA. The correlation profile along the depth direction is given by:

$$\rho[n] = \frac{\sum_{k=1+(n-1)\Delta}^{L_0}\left(S_1[k]-\overline{S}_{1n}\right)\cdot\left(S_2[k]-\overline{S}_{2n}\right)}{\sqrt{\sum_{k=1+(n-1)\Delta}^{L_0}\left(S_1[k]-\overline{S}_{1n}\right)^2\cdot\sum_{k=1+(n-1)\Delta}^{L_0}\left(S_2[k]-\overline{S}_{2n}\right)^2}},$$
$$n = 1,\ldots,\frac{N-L_w}{\Delta}+1, \quad \Delta = L^w - L^0, \tag{12}$$

where S_1 and S_2 are the amplitudes of RF signals before and after microbubble fragmentation, respectively; k denotes the sample number along the depth direction; n is the window number; N is the total number of range samples; L^w represents the number of range samples per window; L^0 is the number of overlapping range samples; and $\overline{S}_{1n}$ and $\overline{S}_{2n}$ are the means of S_1 and S_2 for window n, respectively. The value of ρ is close to 1 when S_1 and S_2 correspond to immovable tissue, and approaches 0 when S_1 and S_2 are from the UCA-rich region. Note that prior to applying this equation, speckle tracking is used to align the image/data across frames/signals so as to reduce motion artifacts.

Fig. 2 gives an example to illustrate the CBA. Figs. 2(a) and (b) show the simulated RF signals before and after microbubble fragmentation in the 25-MHz ultrasound imaging system, respectively. The region within the dashed box in Fig. 2(a) represents the UCA-rich region (i.e., blood perfusion area). The value of ρ is calculated using (12) with a window size of 160 μm and a sliding window with 90% overlap. Note that the window size is determined by the spatial resolution of the imaging transducer. Fig. 2(c) shows the correlation-coefficient profile along the depth direction. A threshold value is essential to separating the perfusion area from tissue background, with the area below the threshold being considered to be the blood perfusion area. Selecting the appropriate threshold is important because variations in the background noise will influence the accuracy of the perfusion-area location if the threshold is either too high or too low. In this study, the threshold value was determined by analyzing a series of simulation data with signal-to-noise ratios (SNRs) ranging from 10 to 50 dB. For the results presented here, we used a threshold of 0.8, which provided over 90% location accuracy under different SNR conditions.

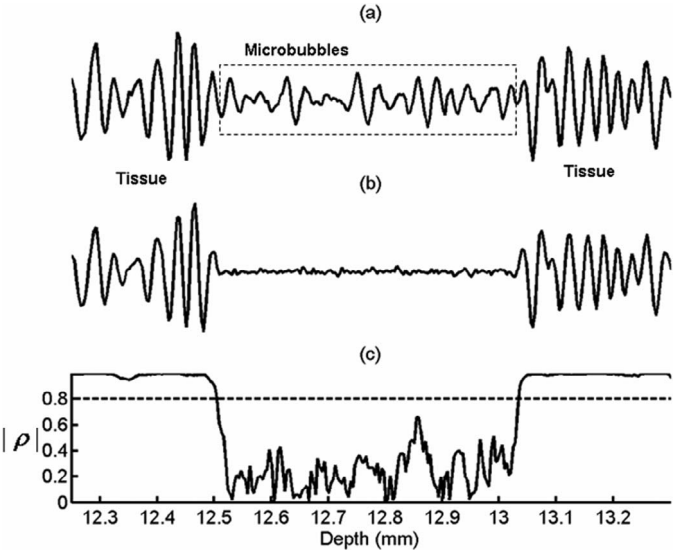

Fig. 2. Simulated RF signals before (a) and after (b) microbubbles fragmentation, and (c) correlation-coefficient profile along depth direction.

III. Results

A. Simulation Model

Computer simulations were used to model the TICs. The adopted simulation model was that proposed by Kerr and Hunt [32]. The original application of this simulator was to emulate ultrasound Doppler color flow images. In our technique we do not excite substantial nonlinear modes of oscillation. Instead we detect the microbubbles based on their strong backscattered echoes and movement through the microvasculature. The model assumed that microbubbles and surrounding tissue represent two-dimension distributions of point-like scatterers. Because microbubble echoes are detected by the high-frequency transducer at far above their linear resonance frequencies, we assumed that the microbubbles behave as Rayleigh scatterers. The acoustic response of each scatterer positioned in the acoustic field was calculated based on its acoustic impulse response. The amplitude of the backscattered signal ($V(t)$) from stationary scatterers can be represented as:

TABLE I
IMAGING TRANSDUCER CHARACTERISTICS.

Central frequency	25 MHz
Element diameter	6.35
Focal length	12.70
−6 dB bandwidth	60%
−6 dB depth of focus	1.50
−6 dB elevational beam width	0.11

(Units: mm)

$$V(t) = P_e(t) * \sum_{i=1}^{N} \kappa_i h_t(\vec{r}_i, t) * h_r(\vec{r}, t), \qquad (13)$$

where $P_e(t)$ is the Gaussian pulse/echo response; $h_t(\vec{r}, t)$ and $h_r(\vec{r}, t)$ are the transmit and receive acoustic impulse responses, respectively; $\vec{r}_i$ is the position of the ith scatterer; N is the total number of scatterers; and κ_i denotes the scale factor for the ith scatterer.

B. Simulation Results

The parameters of the 25-MHz transducer used for microbubble-replenishment imaging are given in Table I. The imaging pulses were transmitted with a pulse repetition frequency (PRF) of 1 kHz, and the microbubbles were modeled as moving in a direction perpendicular to the elevational plane. In order to simulate the flow randomization in the microcirculation, microbubbles were modeled as moving forward with time-varying flow velocities and directions. Before microbubble replenishment, the microbubbles were orderly distributed outside the imaging sample volume (i.e., the boundary of the −6-dB elevational beam width), as shown in Fig. 3(c). After microbubble replenishment, their velocities were normally distributed with a mean of 1 mm/s and a standard deviation of 0.5 mm/s. Random backscattering coefficients were used to simulate microbubbles of different sizes in the microcirculation. The backscattering coefficients were normally distributed with a mean of 1 and a standard deviation of 0.3. Figs. 3(d) and (e) show diagrams of the microbubble distribution when the microbubble concentration was restored to 50% in the sample volume (t_1) and in the entire (t_2) sample volume, respectively. The solid line in Fig. 3(a) represents the final simulated TIC.

The ITIC corresponding to a raw TIC is shown as a solid line in Fig. 3(b). The ITICs were calculated by integrating the raw TICs and fitting them to a model based on (10) to obtain the estimate of A, which was obtained using linear fitting to the last 50 samples of the ITIC, corresponding to the last 0.05 s in the TIC ($t = 0.2$ to $t = 0.25$ s). With the estimated value of A from (10), the estimates of α and c can be jointly obtained from curve fitting to the ITIC model in (11). The dashed line in Fig. 3(b) represents the resulting fitted ITIC. The correlation coefficient (R) between the two curves was 0.96. The dashed line in Fig. 3(a) shows the fit to the sigmoid-based TIC from (2)

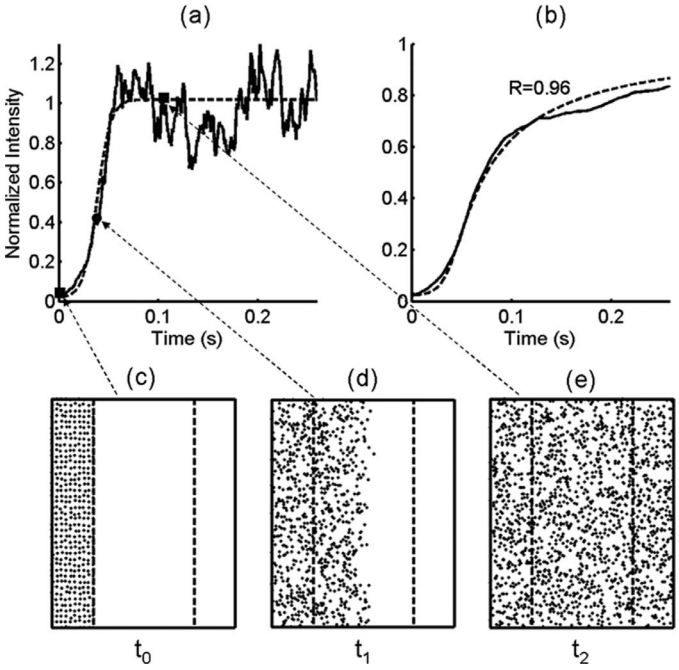

Fig. 3. (a) Simulated raw TIC of flow randomization (solid line) and sigmoid-based fitting curve (dashed line). (b) ITIC of raw TIC (solid line), and ITIC fitting curve (dashed line). (c)–(e) Diagrams of the time course of microbubble replenishment through the imaging plane.

for the estimates of A, α, and c, with the o symbol denoting the inflection point. The results indicate that the TIC predicted by the sigmoid-based model provides a reasonable fit to the simulated raw TIC in the case of flow randomization.

The random-flow cases for mean flow velocities of 3, 5, and 10 mm/s and a standard deviation of 0.5 mm/s are shown in Fig. 4. The simulated raw TICs are shown in Figs. 4(a)–(c) as solid lines. Using the estimated values of A, α, and c obtained from fits to (10) and (11), fits to the TICs from (2) are plotted as dashed lines in Figs. 4(a)–(c). The estimates of α and $1/c$ for different mean flow velocities are shown in Figs. 4(d) and (e), respectively. The actual mean flow velocities were linearly related to the estimates of both α ($R = 0.95$) and $1/c$ ($R = 0.93$).

C. Results of In Vitro Experiments

Because M-mode images provide better temporal resolution than B-mode images in TIC analyses, M-mode imaging microbubble-destruction/replenishment experiments were used to validate the proposed sigmoid-based model. However, B-mode imaging experiments were used to measure the volumetric flow.

1. Experimental Setup: Fig. 5 shows a block diagram of the experimental setup. A dialysis tube with an inner diameter of 1.09 mm was embedded inside an agar phantom constructed by dissolving 2 g of agarose powder in 100 mL of water. The commercial UCA Definity® (Bristol-Myers Squibb Medical Imaging Inc., N. Billerica, MA) was used at 0.6 mL per liter of water. The flow rate was controlled by

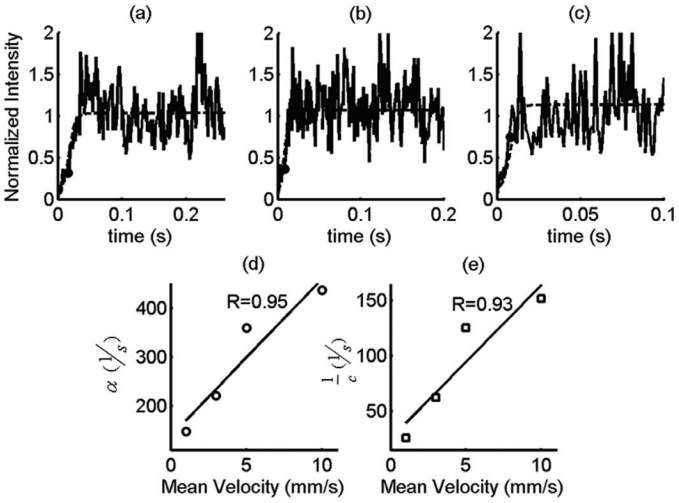

Fig. 4. (a)–(c) Simulated raw TICs (solid lines) and sigmoid-based fitting curves (dashed lines) of flow randomization cases for mean flow velocities of 3, 5, and 10 mm/s, respectively. (d) and (e) show the estimates of α and $1/c$, respectively.

TABLE II
DESTRUCTION TRANSDUCER CHARACTERISTICS.

Central frequency	1 MHz
Element diameter	12.70
Focal length	18.40
−6 dB bandwidth	72%
−6 dB depth of focus	14.52
−6 dB elevational beam width	3.60

(Units: mm)

a syringe pump. A magnetic stir bar inside the syringe was used to keep the solution well mixed. The system consisted of two single-element transducers with spherical foci. A 25-MHz transducer (model V324, GE Panametrics, Waltham, MA) was used for high-resolution imaging, and a 1-MHz transducer (model V303, GE Panametrics) was used for bubble destruction. The specifications of the transducers are summarized in Tables I and II. The two transducers were fixed in a machined holder in a confocal arrangement. The 25-MHz imaging elevational plane was aligned perpendicular to the flow axis of the flow phantom.

The pulser/receiver (model 5900PR, GE Panametrics) provided impulse excitation to the 25-MHz transducer and received the RF signal through a transformer diplexer/diode limiter circuit. The excitation energy was 8 μJ, which produced an acoustic pressure of 0.24 MPa at the transducer focus based on the hydrophone measurements. The received RF signal was amplified by a low-noise preamplifier (model AU-1114-BNC, Miteq, Hauppauge, NY), then further amplified by 42 dB within the pulser/receiver. The RF echoes were digitized at 120 Msamples/s using a PC-based 14-bit analog-to-digital board (model PCI-9820, AdLink, Taipei, Taiwan) and stored on the computer for offline processing.

The 1-MHz destruction pulses with a length of 10 cycles were generated by a programmable arbitrary-waveform generator (model 5300, Tabor Electronics, Tel Hanan, Israel), then amplified by an RF power amplifier (model 150A100B, AR, Bothell, WA) to produce an acoustic pressure of 0.7 MPa at the transducer focus. In our previous study, we found that over 95% of the microbubbles can be destroyed by 10 cycles of a 1-MHz pulse at 0.6 MPa [33].

The transistor-transistor logic (TTL) triggers for 25- and 1-MHz pulse sequences were generated by an analog-to-digital-board standard sampling clock and synchronized to it using a counter/timer board (PCI-6602, National Instruments, Austin, TX). The 1-MHz transducer was switched on after imaging pulses had been transmitted for 1 s. To ensure that all the microbubbles within the sample volume were completely fragmented, the destruction pulses were transmitted with a PRF of 1 kHz for 1 s.

2. Experimental Results from M-Mode Imaging: A typical M-mode image for a flow rate of 1.4 mL/hour (i.e., 0.42 mm/s mean velocity) is shown in Fig. 6(a) with a dynamic range of 50 dB. A parabolic flow profile is evident inside the tube. The 25-MHz imaging pulse was transmitted with a PRF of 1 kHz. Because the UCA destruction volume is larger than the imaging volume, intact microbubbles were replenished in the sample volume after a short delay. The raw TIC [solid line in Fig. 6(b)] was obtained by summing the intensities of the backscattered echoes along the depth direction as a function of time. The corresponding ITIC was obtained by integrating the raw TIC [solid line in Fig. 6(c)]. The resulting fitting ITIC based on (10) and (11) is shown as the dashed-dotted line in Fig. 6(c). The dashed line in Fig. 6(b) shows the fit to the sigmoid-based TIC from (2) for the estimates of A, α, and c obtained from (10) and (11). The o symbol in Fig. 6(b) represents the inflection point of the sigmoid-based model. For comparison with the monoexponential model of Wei *et al.* [20], the monoexponential-based fits of TIC and ITIC are plotted as dotted lines in Figs. 6(b) and (c), respectively. The detailed fitting process of the mono-exponential model is available elsewhere [30]. The experimental results show that the microbubble-replenishment process is described more accurately by our proposed sigmoid-based model than by the monoexponential-based model.

The solid lines in Figs. 7(a)–(c) show the raw TICs for mean flow velocities ranging from 0.85 to 1.70 mm/s in M-mode imaging experiments (corresponding to flow rates from 1.4 to 7.3 mL/h). The dashed lines in Figs. 7(a)–(c) show the fits to the sigmoid-based TICs from (2) for the estimates of A, α, and c, with the square symbols denoting the inflection points. The estimates of α and $1/c$ shown in Figs. 7(d) and (e), respectively, indicating that they are linearly related to the actual flow velocity ($R = 0.97$ and 0.98, respectively).

3. Microcirculation Volumetric Flow Assessment from B-Mode Imaging Experiments: A flow phantom capable of generating the very low flow velocities typically found in the microcirculation (0.1–5 mm/s) was developed [30]. The flow phantom consisted of a 5-mm diameter flow tube, into

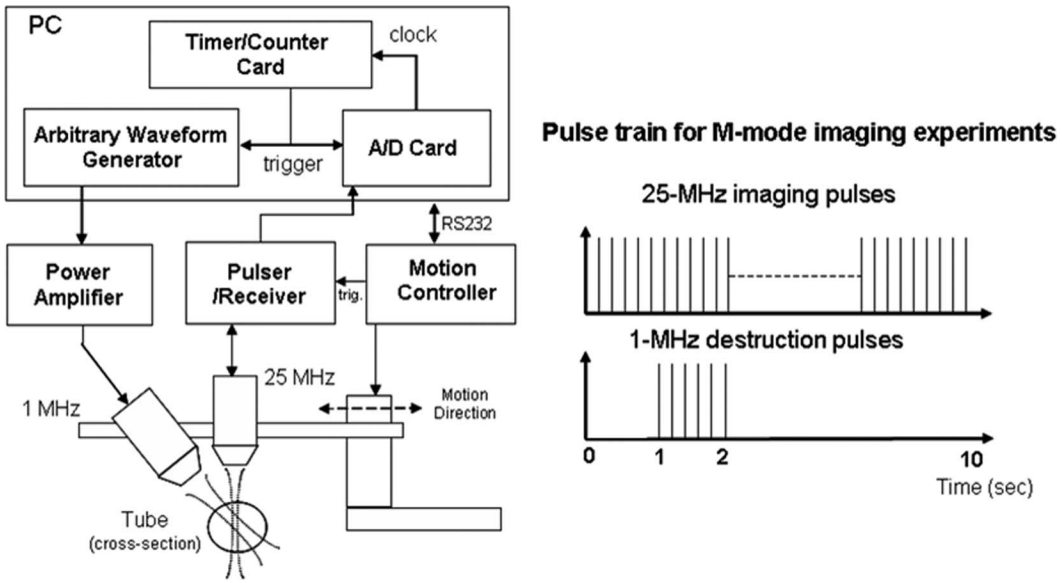

Fig. 5. A block diagram of microbubbles-destruction/replenishment experimental setup and pulse train for the M-mode imaging experiments. The 25-MHz imaging elevational plane was aligned perpendicular to the phantom flow axis.

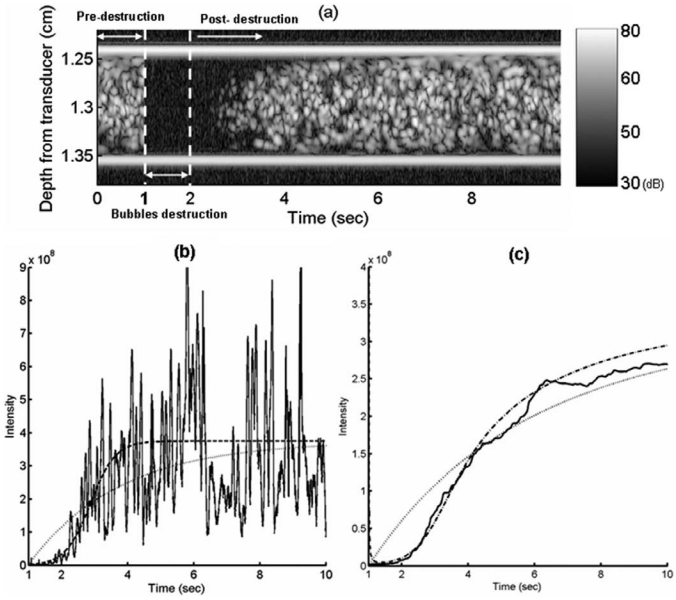

Fig. 6. (a) Typical M-mode image of microbubbles-destruction/replenishment experiment. (b) Raw TIC (solid line), sigmoid-based fitting curve (dashed line), and monoexponential-based model fitting curve (dotted line). (c) ITIC of raw TIC (solid line), ITIC fitting by sigmoid-based model (dash-dot line), and ITIC fitting by monoexponential-based model (dotted line).

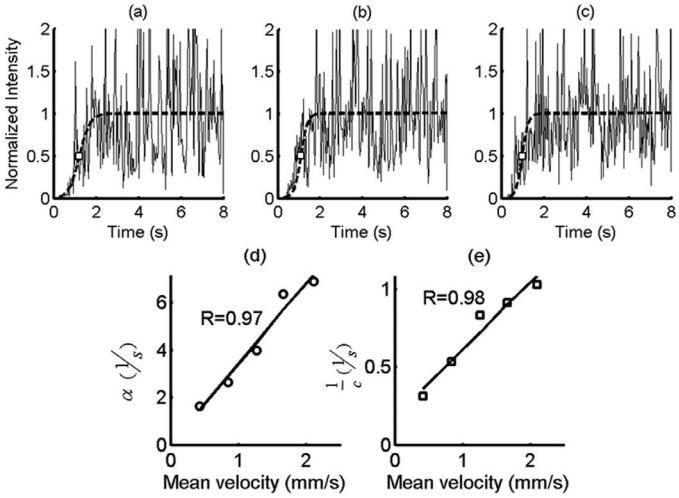

Fig. 7. (a)–(c) Raw TICs (solid lines) and sigmoid-based fitting curves (dashed lines) for mean flow velocities of 0.85, 1.27, and 1.70 mm/s, respectively. The estimates of α and $1/c$ are shown in (d) and (e), respectively.

which a small amount of cotton was placed to emulate tissue scattering and produce flow randomization. Definity® at 0.6 μL/L in water was used as the UCA, and steady flow rates of 30–300 mL/h were produced by a syringe pump.

The system setup is similar for B- and M-mode imaging experiments. In B-mode imaging, the transducer holder was fixed to a high-speed three-dimensional (3-D) motion stage (model HR8, Nanomotion, Yokneam, Israel) for high-speed image scanning. A motion controller (DMC-2140, Galil Motion Control, Rocklin, CA) and a data acquisition system were controlled by software running on a computer. The B-mode images were 1.8 mm deep and 1 mm wide. They were acquired at a frame rate of approximately 10 fps. A total of 100 frames were acquired, with the first frame obtained immediately before microbubble destruction and 99 frames obtained after microbubble destruction. Speckle tracking was applied to ensure image alignment across frames to reduce motion artifacts when imaging with a mechanically scanned transducer. Fig. 8(a) shows the frame obtained prior to bubble destruction. The first frame after bubble destruction is shown in Fig. 8(b). In this case, the flow rate was 90 mL/h (i.e., 1.27 mm/s).

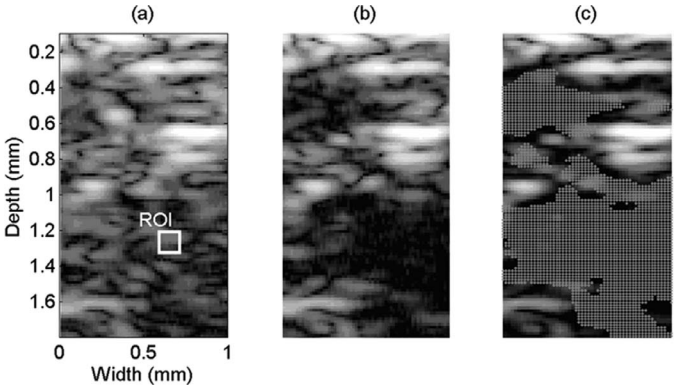

Fig. 8. The *in vitro* experimental B-mode images before (a) and after (b) microbubbles fragmentation and the located perfusion area (denoted by gray dots) in (c).

4. Locating the Perfusion Area: In Figs. 8(a) and (b), a sliding and 90% overlapping kernel block of size 160×160 μm was used to locate the presence of microbubbles by means of the CBA. Image blocks lower than the threshold value of 0.8 were assigned to the blood perfusion area. The gray pixels in Fig. 8(c) show the located perfusion area. Each pixel in the image is 256 μm^2. Hence, the total estimated perfusion area is 0.49 mm^2 in this case.

5. Estimation of Volumetric Flow Rate: An ROI within the perfusion area shown in Fig. 8(a) of size 160×160 μm was selected to illustrate the TIC in B-mode imaging experiments. The raw TIC and sigmoid-based fitted TIC from the ITIC are shown as solid and dashed lines in Fig. 9(a), respectively. The corresponding ITIC of the raw TIC is shown as the solid line in Fig. 9(b), and the dashed line shows the ITIC fitted using (10) and (11). The results of estimates of α and $1/c$ with mean flow velocities ranging from 0.42 to 2.12 mm/s are shown in Figs. 9(c) and (d), respectively. For each flow rate, five independent experimental estimates of α and $1/c$ were used to calculate the mean and standard deviation. The actual flow velocity was highly linearly related to both α ($R = 0.99$) and $1/c$ ($R = 0.99$) within the selected ROI.

The flow velocity of the located perfusion area [as in Fig. 8(c)] could be mapped using the same signal processing as described above. Accordingly, the volumetric flow rates calculated by multiplying the located perfusion area and the corresponding estimates of α and $1/c$ are shown in Figs. 9(e) and (f), respectively. Highly linear relationships ($R = 0.98$) are evident in both cases. Eq. (5) indicates that the value of $1/c$ is half that of α. In other words, the flow rate estimates obtained from $\alpha \times PA$ should be twice those of $1/c \times PA$. However, the results shown in Figs. 9(e) and (f) are not consistent with this. This discrepancy might be due to the uncertainty in the boundary of the actual volume in which microbubbles are destroyed. Eqs. (3)–(6) were theoretically derived based on the bubble replenishment at the boundary of the −6-dB elevational beam width. The microbubble fragmentation volume varies with the sonication parameters of the destruction pulses and the concentration at which bubbles are infused.

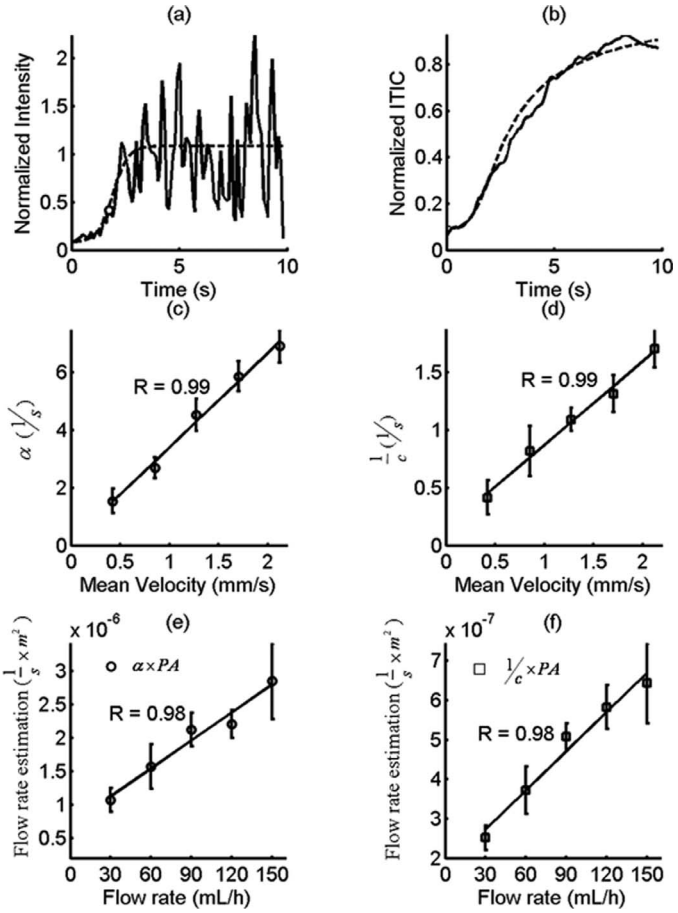

Fig. 9. (a) Raw TIC (solid line) of the selected ROI in Fig. 8(a) and sigmoid-based fitting curve (dashed line). (b) ITIC of raw TIC (solid line) and ITIC fitting curve (dashed line). The (c) and (d) show the resulting estimates of α and $1/c$, respectively. The (e) and (f) show the assessment of volumetric flow rate by $\alpha \times PA$ and $1/c \times PA$, respectively.

IV. Conclusions

Fig. 1 shows that the TIC appears as a rising exponential curve after the inflection point when the flow velocity is very high. If the imaging sample volume contains vessels with varying flow velocities, the resultant TIC can be viewed as the linear combination of the respective TICs for different flow velocities. This circumstance can be simulated by summing the TICs of the respective flow velocities, as shown in Figs. 4(a)–(c), which results in an approximate monoexponential-type TIC (which is shown as a solid line in Fig. 10; the dotted line represents the fitted curve for the monoexponential-based model). In other words, the use of lower frequency ultrasound might result in a TIC with an exponential shape due to its larger sampling volume containing vessels with a larger range of flow velocities. Conversely, because the sample volume of high-frequency ultrasound is smaller, the vessel sizes and corresponding flow velocities will be more uniform. There-

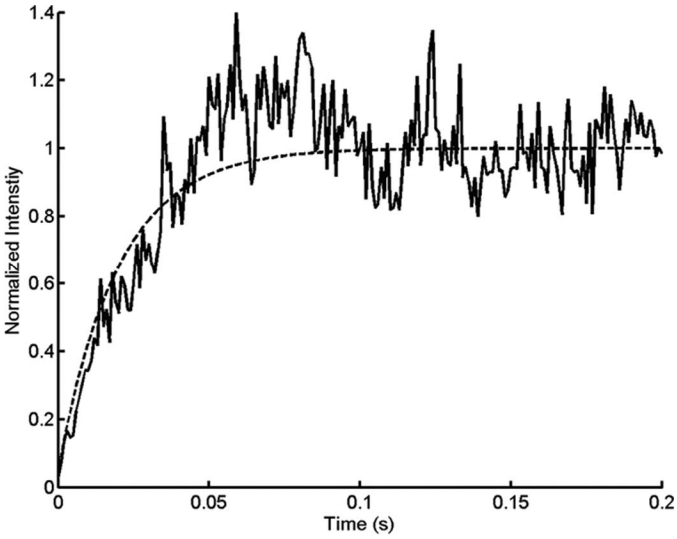

Fig. 10. Summation of the simulated TICs as illustrated in Figs. 4(a)–(c) (solid line) and monoexponential-based model fitting curve (dashed line).

fore, the above-mentioned circumstance may not occur in the case of high-frequency ultrasound.

We previously constructed a 25-MHz UCA-destruction/replenishment imaging system with a spatial resolution of 160×160 μm. This was used here to propose a new approach for functionally evaluating the microvascular volumetric blood flow. The approach includes locating the perfusion area and estimating the blood flow velocity therein. Because the correlation changes between before and after microbubble destruction in two adjacent images, a CBA was introduced to detect the presence of UCAs (i.e., the blood perfusion area). Note that the technique for locating the perfusion area becomes invalid in the presence of vessels that are smaller than the kernel block size (i.e., the ultrasound spatial resolution).

We also have derived a new sigmoid-based model for characterizing the UCA replenishment process. This was validated using both simulations and *in vitro* experiments, which showed that the model was in good agreement with experimentally measured microbubble-replenishment TICs. The rate constant and inflection time derived from the sigmoid-based model are used to evaluate the blood flow velocity. The results indicate that the actual flow velocity is highly correlated with the estimates of the rate constant and the reciprocal of the inflection time.

B-mode imaging experiments were used to assess the volumetric flow in the microcirculation. A flow phantom constructed to simulate the very low flow rates of the microcirculation indicated the high correlation between the actual volumetric flow rate and the product of the estimated perfusion area and rate constant, and the reciprocal of the inflection time. We also found that the boundary of the microbubble destruction volume significantly affected estimations of the flow velocity.

The perfusion area can be located and the corresponding flow velocity can be estimated simultaneously in a one-stage microbubble-destruction/replenishment process, which makes the assessment of the volumetric blood flow in the microcirculation feasible using a real-time high-frequency ultrasound system. Potential applications of this method include the high-resolution assessment of tumor volumetric blood flow in small animals and the evaluation of the superficial vasculature in clinical studies.

References

[1] N. Weidner, J. P. Semple, W. R. Welch, and J. Folkman, "Tumor angiogenesis and metastasis-correlation in invasive breast carcinoma," *New Engl. J. Med.*, vol. 324, pp. 1–7, 1991.

[2] R. Folberg, J. Pe'er, and L. M. Gruman, "The morphologic characteristics of tumor blood vessels as a marker of tumor progression in primary human uveal melanoma: A matched case-control study," *Hum. Pathol.*, vol. 23, pp. 1298–1305, 1992.

[3] T. Makitie, P. Summanen, A. Tarkkanen, and T. Kivela, "Microvascular density in predicting survival of patients with choroidal and ciliary body melanoma," *Invest. Ophthalmol. Vis. Sci.*, vol. 40, pp. 2471–2480, 1999.

[4] Y. C. Fung, *Biomechanics: Circulation*. New York: Springer-Verlag, 1997.

[5] A. C. Guyton and J. E. Hall, *Human Physiology and Mechanisms of Disease*. Philadelphia: W. B. Saunders, 1997.

[6] D. H. Turnbull, B. G. Starkoski, K. A. Harasiewicz, J. L. Semple, L. From, A. K. Gupta, D. N. Sauder, and F. S. Foster, "A 40–100 MHz B-scan ultrasound backscatter microscope for skin imaging," *Ultrasound Med. Biol.*, vol. 21, pp. 79–88, 1995.

[7] C. J. Pavlin and F. S. Foster, "Ultrasound biomicroscopy high-frequency ultrasound imaging of the eye at microscopic resolution," *Radiol. Clin. North Amer.*, vol. 36, pp. 1047–1058, 1998.

[8] R. H. Silverman, F. L. Lizzi, B. G. Ursea, M. J. Rondeau, N. B. Eldeen, A. Kaliscz, H. O. Lloyd, and D. J. Coleman, "High-resolution ultrasonic imaging and characterization of the ciliary body," *Invest. Ophthalmol. Vis. Sci.*, vol. 42, pp. 885–894, 2001.

[9] O. Aristizabal, D. A. Christopher, F. S. Foster, and D. H. Turnbull, "40-MHz echocardiography scanner for cardiovascular assessment of mouse embryos," *Ultrasound Med. Biol.*, vol. 24, pp. 1407–1417, 1998.

[10] D. E. Kruse, R. H. Silverman, R. J. Fornaris, D. J. Coleman, and K. W. Ferrara, "A swept-scanning mode for estimation of blood velocity in the microvasculature," *IEEE Trans. Ultrason., Ferroelect., Freq. Contr.*, vol. 45, pp. 1437–1440, 1998.

[11] D. E. Goertz, D. A. Christopher, J. L. Yu, R. S. Kerbel, P. N. Burns, and F. S. Foster, "High-frequency color flow imaging of the microcirculation," *Ultrasound Med. Biol.*, vol. 26, pp. 63–71, 2000.

[12] D. E. Kruse and K. W. Ferrara, "A new high resolution color flow system using an eigendecomposition-based adaptive filter for clutter rejection," *IEEE Trans. Ultrason., Ferroelect., Freq. Contr.*, vol. 49, pp. 1384–1399, 2002.

[13] J. E. Chomas, P. Dayton, J. Allen, K. Morgan, and K. W. Ferrera, "Mechanisms of contrast agent destruction," *IEEE Trans. Ultrason., Ferroelect., Freq. Contr.*, vol. 48, pp. 232–248, 2001.

[14] J. E. Chomas, P. Dayton, D. May, and K. Ferrara, "Threshold of fragmentation for ultrasonic contrast agents," *J. Biomed. Opt.*, vol. 6, pp. 141–150, 2001.

[15] J. E. Chomas, P. Dayton, D. May, J. Allen, A. Klibanov, and K. Ferrara, "Optical observation of contrast agent destruction," *Appl. Phys. Lett.*, vol. 77, pp. 1056–1058, 2000.

[16] P. J. Frinking, E. L. Cespedes, J. Kirkhorn, H. G. Torp, and N. de-Jong, "A new ultrasound contrast imaging approach based on the combination of multiple imaging pulses and a separate release burst," *IEEE Trans. Ultrason., Ferroelect., Freq. Contr.*, vol. 48, pp. 643–645, 2001.

[17] K. Wei, A. R. Jayaweera, S. Firoozan, A. Linka, D. M. Skyba, and S. Kaul, "Quantification of myocardial blood flow with ultrasound-induced destruction of microbubbles administered as a constant venous infusion," *Circulation*, vol. 97, pp. 473–483, 1998.

[18] H. Masugata, B. Peters, S. Lafitte, G. M. Strachan, K. Ohmori, and A. N. DeMaria, "Quantitative assessment of myocardial per-

fusion during graded coronary stenosis by real-time myocardial contrast echo refilling curves," *J. Amer. Coll. Cardiol.*, vol. 37, pp. 262–269, 2001.
[19] A. Oshita, K. Ohmori, Y. Yu, I. Kondo, H. Takeuchi, Y. Takagi, Y. Wada, K. Yukiiri, K. Mizushige, and M. Kohno, "Myocardial blood flow measurements in rats with simple pulsing contrast echocardiography," *Ultrasound Med. Biol.*, vol. 28, pp. 459–466, 2002.
[20] K. Wei, E. Le, J. P. Bin, M. Coggins, J. Thorpe, and S. Kaul, "Quantification of renal blood flow with contrast-enhanced ultrasound," *J. Amer. Coll. Cardiol.*, vol. 37, pp. 1135–1140, 2001.
[21] S. J. Rim, H. Leong-Poi, J. R. Lindner, D. Couture, D. Ellegala, H. Mason, M. Durieux, N. F. Kassel, and S. Kaul, "Quantification of cerebral perfusion with real-time contrast-enhanced ultrasound," *Circulation*, vol. 104, pp. 2582–2587, 2001.
[22] G. Seidel and K. Meyer, "Harmonic imaging: A new method for the sonographic assessment of cerebral perfusion," *Eur. J. Ultrasound*, vol. 14, pp. 103–113, 2001.
[23] G. Seidel, L. Claassen, K. Meyer, and M. V. Langwasser, "Evaluation of blood flow in the cerebral microcirculation: Analysis of the refill kinetics during ultrasound contrast agent infusion," *Ultrasound Med. Biol.*, vol. 27, pp. 1059–1064, 2001.
[24] J. E. Chomas, P. Dayton, D. May, and K. Ferrara, "Nondestructive subharmonic imaging," *IEEE Trans. Ultrason., Ferroelect., Freq. Contr.*, vol. 49, pp. 883–892, 2002.
[25] T. Schlosser, C. Pohl, C. Veltmann, S. Lohmaier, J. Goenechea, A. Ehlgen, J. Koster, D. Bimmel, S. Kunta-Henner, H. Becher, and K. Tiemann, "Feasibility of the flash-replenishment concept in renal tissue: Which parameters affect the assessment of the contrast replenishment?," *Ultrasound Med. Biol.*, vol. 27, pp. 937–944, 2001.
[26] O. Lucidarme, S. Franchi-Abella, J. M. Correas, S. L. Bridal, E. Kurtisovski, and G. Berger, "Blood flow quantification with contrast-enhanced US: Entrance in the section phenomenon-phantom and rabbit study," *Radiology*, vol. 228, pp. 473–479, 2003.
[27] J. M. Hudson, R. Karshafian, and P. N. Burns, "Quantification of flow using ultrasound and microbubbles: A disruption replenishment model based on physical principles," in *Proc. IEEE Ultrason. Symp.*, 2006, pp. 1588–1591.
[28] M. Arditi, P. J. Frinking, X. Zhou, and N. G. Rognin, "A new formalism for the quantification of tissue perfusion by the destruction-replenishment method in contrast ultrasound imaging," *IEEE Trans. Ultrason., Ferroelect., Freq. Contr.*, vol. 53, pp. 1118–1129, 2006.
[29] M. Krix, F. Kiessling, N. Farhan, K. Schmidt, J. Hoffend, and S. Delorme, "A multivessel model describing replenishment kinetics of ultrasound contrast agent for quantification of tissue perfusion," *Ultrasound Med. Biol.*, vol. 29, pp. 1421–1430, 2003.
[30] C. K. Yeh, K. W. Ferrara, and D. E. Kruse, "High-resolution functional vascular assessment with ultrasound," *IEEE Trans. Med. Imag.*, vol. 23, pp. 1263–1275, 2004.
[31] C. K. Yeh, S. Y. Lu, and W. S. Chen, "The correlation-based algorithm to perfusion assessment in ultrasound image," in *Proc. IEEE Eng. Med. Biol.*, 2005, pp. 3233–3236.
[32] T. Kerr and J. W. Hunt, "A method for computer simulation of ultrasound Doppler color flow images—I. Theory and numerical method," *Ultrasound Med. Biol.*, vol. 18, pp. 861–872, 1992.
[33] C. K. Yeh, S. Y. Su, and W. S. Chen, "Destruction threshold parameters estimation for ultrasonic contrast agents," *J. Med. Biol. Eng.*, vol. 25, pp. 167–171, 2005.

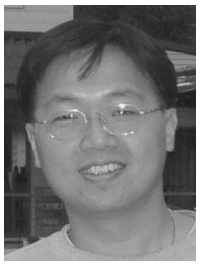

Chih-Kuang Yeh was born in 1973 in Taiwan, R.O.C. He received his B.S., M.S., and Ph.D. degrees in biomedical engineering from Chung-Yuan Christian University, Chung-Li, Taiwan, in 1995 and National Cheng-Kung University, Tainan, Taiwan, in 1997, and in electrical engineering from National Taiwan University, Taipei, Taiwan in 2004, respectively. He joined Professor Katherine Ferrara's research group in the University of California at Davis as a visiting researcher from 2003 to 2004. In 2005, he joined the Department of Biomedical Engineering and Environmental Sciences, National Tsing Hua University, Hsinchu, Taiwan. He now is an assistant professor.

His current research interests include ultrasound contrast agents and ultrasonic flow velocity estimation.

Sheng-Yi Lu was born in 1981 in Taiwan, R.O.C. He received his B.S. and M.S. degrees in electrical engineering from Yuan Ze University, Chung-Li, Taiwan in 2004 and 2006, respectively.

His research interests are ultrasound contrast agents and blood flow estimation.

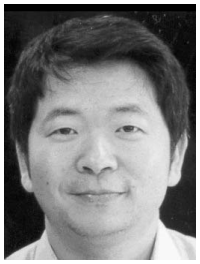

Yung-Sheng Chen was born in Taiwan, R.O.C., on June 30, 1961. He received the B.S. degree from Chung Yuan Christian University, Chung-Li, Taiwan, in 1983 and the M.S. and Ph.D. degrees from National Tsing Hua University, Hsinchu, Taiwan, in 1985, and 1989, respectively, all in electrical engineering. In 1991, he joined the Electrical Engineering Department, Yuan Ze Institute of Technology, Chung-Li, Taiwan, where he is now a professor.

His research interests include human visual perception, computer vision and graphics, circuit design, and website design.

Dr. Chen received the Best Paper Award from the Chinese Institute of Engineers in 1989 and an Outstanding Teaching Award from Yuan Ze University in 2005. He has been listed in the Who's Who of the World since 1998 and awarded with The Millennium Medal from The Who's Who Institute in 2001. He is a member of the IEEE, and the IPPR of Taiwan, R.O.C.